TU/e EINDHOVEN UNIVERSITY OF TECHNOLOGY

Multiscale modeling of colloidal dynamics in porous media : capturing aggregation and deposition effects

Citation for published version (APA):
Krehel, O., Muntean, A., & Knabner, P. (2014). *Multiscale modeling of colloidal dynamics in porous media : capturing aggregation and deposition effects*. (CASA-report; Vol. 1412). Technische Universiteit Eindhoven.

Document status and date:
Published: 01/01/2014

Document Version:
Publisher's PDF, also known as Version of Record (includes final page, issue and volume numbers)

Please check the document version of this publication:

• A submitted manuscript is the version of the article upon submission and before peer-review. There can be important differences between the submitted version and the official published version of record. People interested in the research are advised to contact the author for the final version of the publication, or visit the DOI to the publisher's website.
• The final author version and the galley proof are versions of the publication after peer review.
• The final published version features the final layout of the paper including the volume, issue and page numbers.

Link to publication

General rights
Copyright and moral rights for the publications made accessible in the public portal are retained by the authors and/or other copyright owners and it is a condition of accessing publications that users recognise and abide by the legal requirements associated with these rights.

• Users may download and print one copy of any publication from the public portal for the purpose of private study or research.
• You may not further distribute the material or use it for any profit-making activity or commercial gain
• You may freely distribute the URL identifying the publication in the public portal.

If the publication is distributed under the terms of Article 25fa of the Dutch Copyright Act, indicated by the "Taverne" license above, please follow below link for the End User Agreement:

www.tue.nl/taverne

Take down policy
If you believe that this document breaches copyright please contact us at:

openaccess@tue.nl

providing details and we will investigate your claim.

Download date: 17. Nov. 2023

EINDHOVEN UNIVERSITY OF TECHNOLOGY
Department of Mathematics and Computer Science

CASA-Report 14-12
April 2014

Multiscale modeling of colloidal dynamics in porous media: Capturing aggregation and deposition effects

by

O. Krehel, A. Muntean, P. Knabner

Centre for Analysis, Scientific computing and Applications
Department of Mathematics and Computer Science
Eindhoven University of Technology
P.O. Box 513
5600 MB Eindhoven, The Netherlands
ISSN: 0926-4507

Multiscale Modeling of Colloidal Dynamics in Porous Media: Capturing Aggregation and Deposition Effects

Oleh Krehel

Department of Mathematics and Computer Science
CASA - Center for Analysis, Scientific computing and Engineering
Eindhoven University of Technology
5600 MB, PO Box 513, Eindhoven, The Netherlands

Adrian Muntean

Department of Mathematics and Computer Science
CASA - Center for Analysis, Scientific computing and Engineering
ICMS - Institute for Complex Molecular Systems
Eindhoven University of Technology
5600 MB, PO Box 513, Eindhoven The Netherlands

Peter Knabner

Department of Mathematics
Friedrich-Alexander University of Erlangen-Nuremberg
Cauerstr. 11, Erlangen 91058, Germany

Abstract

We investigate the influence of multiscale aggregation and deposition on the colloidal dynamics in a saturated porous medium. At the pore scale, the aggregation of colloids is modeled by the Smoluchowski equation. Essentially, the colloidal mass is distributed between different size clusters. We treat these clusters as different species involved in a diffusion-advection-reaction mechanism. This modeling procedure allows for different material properties to be varied between the different species, specifically the rates of diffusion, aggregation, deposition as well as the advection velocities. We apply the periodic homogenization procedure to give insight into the effective coefficients of the upscaled model equations. Benefiting from direct access to microstructural information, we capture by means of 2D numerical simulations the effect of aggregation on the deposition rates recovering this way both the blocking and ripening regimes reported in the literature.

1 Introduction

Colloids are particles with size ranging approximately from 1 to 1000 nm in at least one dimension. They play a significant functional role in a number of technological and biological applications, such as waste water treatment, food industry, printing, design of drug delivery; see e.g. Nordbotten and Celia, 2012; Rosenholm, Sahlgren, and Lindén, 2010. The existing literature on colloids and their dynamics is huge. Here we only mention that the self-assembly of collagen structures (basic component of the mechanics of the human body) together with secondary nucleation effects have recently been treated in Lith, Storm, and Muntean, 2013, starting off from an interacting particle system for colloids. A detailed discussion of the main principles of aggregation mechanisms can be found in Peukert, Schwarzer, and Stenger, 2005, while a thorough analysis of the aggregation in terms of ordinary differential equations can be found e.g. in Camejo, Gröpler, and Warnecke, 2012.

The central topic of this paper is the treatment of the aggregation of colloids in porous media (particularly, soils) that has been recently shown to be a dominant factor in estimating contaminant transport; see Totsche and Kögel-Knabner, 2004. Essentially, one supposes that that the presence of colloidal aggregation strongly affects the deposition rates on the pore (grain) boundary. Similar aggregation (group formation, cooperation) patterns can emerge also in pedestrian flows strongly affecting their viscosity Muntean et al., 2014. Previous investigations on contaminant dynamics in soils, yet not accounting explicitly for aggregation, can be found, for instance, in Knabner, Totsche, and Kögel-Knabner, 1996 and Totsche, Knabner, and Kögel-Knabner, 1996.

Our aim here is to study the influence of multiscale aggregation and deposition on the colloidal dynamics in a saturated porous medium mimicking a column experiment performed by Johnson, Sun and Elimelech and reported in Johnson, Sun, and Elimelech, 1996. For more information on this experimental context, we refer the reader also to Refs. Johnson and Elimelech, 1995; Liu, Johnson, and Elimelech, 1995. To get more theoretical insight in this column experiment, we proceed as follows: As departure point, we assume that at the pore scale we can model the aggregation of colloids by the Smoluchowski equation. Consequently, the colloidal mass is distributed between different size clusters. We treat these clusters as different species involved in a coupled diffusion-advection-reaction system. This modeling procedure allows for different material properties to be varied between the different species, specifically the rates of diffusion, aggregation, deposition as well as the advection velocities. As next step, we apply the periodic homogenization methodology to give insight into the effective coefficients of the upscaled model equations. Finally, for a set of reference parameters, we solve the upscaled equations for different choices of microstructures and investigate the influence of aggregation on both transport and deposition of the colloidal mass, validating in the same time our methodology and numerical platform by means of the results from Johnson, Sun, and Elimelech, 1996.

The outline of the paper is as follows: In Section 2 we set up a microscopic

pore-scale model for aggregation, diffusion and deposition of populations of colloidal particles. In Section 3 the microscopic model is nondimensionalized. One of the small dimensionless numbers pointed out therein (denoted by ε) connects a ratio of characteristic time scales of the process to the relevant microscopic and macroscopic length scales arising in the system. In Section 4 we use the concept of two-scale asymptotic expansions to obtain in the limit of small ε an equivalent macroscopic model together with the corresponding effective coefficients. We conclude the paper with a few numerical multiscale experiments and discussions on further work (cf. Section 5 and Section 6).

2 Microscopic model

The foundations of the modeling of colloids aggregation and fragmentation were laid down in the classical work of Smoluchowski Smoluchowski, 1917. A nice overview can be found, for instance, in Elimelech et al., 1995. The role of this section is to introduce our modeling Ansatz on the second order kinetics describing the colloidal cluster growth and decline, the functional structure of the deposition rate, as well as the assumptions on the microscopic diffusion coefficients for the clusters.

2.1 Aggregation and fragmentation of clusters

We assume that the colloidal population consists of identical particles, called primary particles, some of which form aggregate particles that are characterized by the number of primary particles that they contain – i.e. we have u_1 particles of size 1, u_2 particles of size 2, etc. We refer to each particle of size i as a member of the i^{th} species (or of the $i-$cluster).

The fundamental assumption behind this modeling strategy is that aggregation can be perceived as a second-order rate process, i.e. the rate of collision is proportional to concentrations of the colliding species. Thus A_{ij} – the number of aggregates of size $i+j$ formed from the collision of particles of sizes i and j per unit time and volume, equals:

$$A_{ij} := \gamma_{ij} u_i u_j, \text{ with} \tag{1}$$

$$\gamma_{ij} := \alpha_{ij} \beta_{ij}. \tag{2}$$

Here β_{ij} is the collision kernel – rate constant determined by the transport mechanisms that bring the particles in close contact, while $\alpha_{ij} \in [0,1]$ is the collision efficiency – the fraction of collisions that finally form an aggregate. The coefficients α_{ij} are determined by a combination of particle-particle interaction forces, both DLVO (i.e. double-layer repulsion and van der Waals attraction) and non-DLVO, e.g. steric interaction forces (see Derjaguin and Landau, 1941, Hamaker, 1937).

A typical choice for α_{ij} and β_{ij} can be found in for instance in Krehel, Muntean, and Knabner, 2012. The interaction rates (written in the spirit of

balance of populations balances as reaction rates) should then satisfy

$$R_i(u) = \frac{1}{2} \sum_{i+j=k} \alpha_{ij}\beta_{ij}u_i u_j - u_k \sum_{i=1}^{\infty} \alpha_{ki}\beta_{ki}u_i, \tag{3}$$

where $u = (u_1, \ldots, u_N, \ldots)$ is the vector of the concentrations for each size class $i \in \{1, \ldots, N\}$ for a fixed choice of N.

2.2 Diffusion coefficients for clusters

We take the diffusivity d_1 of the monomers as a baseline. All the other diffusivities are here assumed to depend on d_1 in agreement with the Einstein-Stokes relation

$$d_i = \frac{kT}{6\pi\eta r_i}. \tag{4}$$

The cluster diffusion coefficients d_i arising in (4) are designed for the diffusion of spherical particles through liquids at low Reynolds number. In (4), T denotes the absolute temperature, k is the Boltzmann factor, η is the dynamic viscosity, while r_i is the aggregate (i-mer, i-cluster) radius. Note the following dependence of the aggregate radius r_i on the number of monomers contained in the i-cluster:

$$r_i = i^{\frac{1}{D_F}} r_1, \tag{5}$$

with D_F being a dimensionless parameter called the fractal dimension of the aggregate Meakin, 1987. D_F indicates how porous the aggregate is. For instance, a completely non-porous aggregate in three dimensions, such as coalesced liquid drops, would have $D_F = 3$. Combining (4) and (5), we obtain:

$$d_i = \frac{1}{i^{\frac{1}{D_F}}} d_1. \tag{6}$$

2.3 Deposition rate of colloids on grain surfaces

The colloidal species u_i, defined in Ω (see Figure 1), can deposit on the grain boundary of the solid matrix $\Gamma \subset \partial\Omega$, transforming into an immobile species v_i, defined on Γ. This means that the colloids of different size can be present both in the bulk and on the boundary. The boundary condition for Γ then looks like:

$$-d_i \nabla u_i \cdot n = F_i(u_i, v_i). \tag{7}$$

At this stage, we assume the deposition rate F_i to be linear, namely we take

$$F_i(u_i, v_i) = a_i u_i - b_i v_i, \tag{8}$$

this resembles the structure of Henry's law acting in the context of gas exchange at liquid interfaces Battino and Clever, 1966.

2.4 Setting of the microscopic model equations

Collecting the modeling assumptions from Section 2.1, Section 2.2, and Section 2.3, we see that the microscopic system to be tackled in this context is as follows:

Find $(u_1, \ldots, u_N, v_1, \ldots, v_N)$ satisfying

$$\partial_t u_i + \nabla \cdot (-d_i \nabla u_i) = R_i(u) \qquad \text{in } \Omega, \tag{9}$$

$$\partial_t v_i = a_i u_i - b_i v_i \qquad \text{on } \Gamma, \tag{10}$$

with the boundary conditions

$$-d_i \nabla u_i \cdot n = a_i u_i - b_i v_i \qquad \text{on } \Gamma, \tag{11}$$

$$-d_i \nabla u_i \cdot n = 0 \qquad \text{on } \Gamma_N, \tag{12}$$

$$u_i = u_{iD} \qquad \text{on } \Gamma_D, \tag{13}$$

and the initial conditions

$$u_i(0, x) = u_i^0(x) \qquad \text{for } x \in \Omega, \tag{14}$$

$$v_i(0, x) = v_i^0(x) \qquad \text{for } x \in \Gamma. \tag{15}$$

3 Nondimensionalization

Let τ, χ, d, u_0, v_0, and a_0 be reference quantities. We choose the scaling $t := \tau\tilde{t}$, $x := \chi\tilde{x}$, $d_i := d\tilde{d}_i$, $u_i := u_0\tilde{u}_i$, $v_i := v_0\tilde{v}_i$, $a_i := a_0\tilde{a}_i$, and $b_i := \frac{a_0 u_0}{v_0}\tilde{b}_i$. As reference quantities, we select $\chi := L$, $d := d_1$, $u_0 := \max\{u_{i0}, u_{iD} : i \in \{1, \ldots, N\}\}$, and $v_0 := \max\{v_{i0} : i \in \{1, \ldots, N\}\}$.

Note that we need to distinguish between u_0 and v_0 since they have different dimensions, i.e. volume and surface concentration, respectively. After substituting these scaling relations into (9)-(15) and dropping the tildes, we obtain:

$$\partial_t u_i + \frac{\tau d}{L^2} \nabla \cdot (-d_i \nabla u_i) = \tau u_0 R_i(u) \tag{16}$$

$$-d_i \nabla u_i \cdot n = \frac{a_0 L}{d}(a_i u_i - b_i v_i) \tag{17}$$

$$\partial_t v_i = \frac{\tau a_0}{v_0} u_0 (a_i u_i - b_i v_i). \tag{18}$$

This nondimensionalization procedure involves three relevant dimensionless numbers. We denote by ε our first dimensionless number, viz.

$$\varepsilon := \frac{a_0 L}{d}. \tag{19}$$

For our particular scenario, the dimensionless number ε takes a small value (here $\varepsilon \approx 7.61e-7$). We will relate it in Section 4 to a ratio of characteristic micro-macro length scales. We refer to ε as the *homogenization parameter*.

Furthermore, we choose to scale the time variable in the system by the characteristic time scale of diffusion $\tau := \frac{L^2}{d}$ of the fastest species (i.e. the monomers). This particular choice of time scale leads to two further dimensionless numbers:

- the *Thiele modulus*
$$\Lambda := \frac{L^2}{d} u_0 \tag{20}$$
- the *Biot number*
$$Bi := a_0 \frac{L^2}{d} \frac{u_0}{v_0}. \tag{21}$$

According to our reference parameters, we estimate that $\Lambda = 3.8934e21$ and $Bi = 7.6914e-08$. The order of magnitude of the Thiele modulus Λ indicates that the characteristic reaction time is very small compared to the characteristic time of monomers diffusion, the overall reaction-diffusion process being with this scaling in its fast reaction regime. The order of magnitude of the Biot number Bi points out the slow deposition regime. Essentially, since $\frac{Lu_0}{v_0} = \mathcal{O}(1)$, we have $Bi = \mathcal{O}(\varepsilon)$. To remove a proportionality constant in the scaled boundary condition (24), we take $L := \frac{v_0}{u_0}$.

Finally, we obtain the following dimensionless system of governing equations:

$$\partial_t u_i + \nabla \cdot (-d_i \nabla u_i) = \Lambda R_i(u) \qquad \text{in } \Omega, \tag{22}$$
$$\partial_t v_i = Bi(a_i u_i - b_i v_i) \qquad \text{on } \Gamma, \tag{23}$$

with the boundary conditions

$$-d_i \nabla u_i \cdot n = \varepsilon(a_i u_i - b_i v_i) \qquad \text{on } \Gamma, \tag{24}$$
$$-d_i \nabla u_i \cdot n = 0 \qquad \text{on } \Gamma_N, \tag{25}$$
$$u_i(t,x) = \frac{u_D(t,x)}{u_0} \qquad \text{on } \Gamma_D, \tag{26}$$

and the initial conditions

$$u_i(0,x) = \frac{u_i^0(x)}{u_0} \qquad \text{for } x \in \Omega, \tag{27}$$
$$v_i(0,x) = \frac{v_i^0(x)}{v_0} \qquad \text{for } x \in \Gamma. \tag{28}$$

4 Derivation of the macroscopic model

In this section, we suppose that our porous medium has an internal structure that can be sufficiently well approximated by an array of periodically-distributed microstructures. For this situation, starting off from a partly dissipative model for the dynamics of large populations of interacting colloids at the pore level

(i.e. within the microstructure), we derive upscaled equations governing the approximate macroscopically observable behavior. To do this, we employ the technique of periodic homogenization; see, for instance, Bensoussan, Lions, and Papanicolaou, 1978; Chechkin, Piatnitki, and Shamaev, 2007; Marchenko and Kruslov, 2006. In what follows, we apply the technique in an algorithmic way, giving complete and explicit calculations.

4.1 Colloid dynamics in structured media. The periodic homogenization procedure

The porous medium Ω^ε that we consider is modeled here as a composite periodic structure with $\varepsilon > 0$ as a small scale parameter, which relates the the pore length scale to the domain length scale. Ω^ε is depicted in Figure 1. We assume in this context that this scale parameter is of the same order of magnitude as ε introduced in (19). Note in Figure 1 the periodic array of cells approximating the porous media under consideration. Each element is a rescaled (by ε) and translated copy of the standard cell Y.

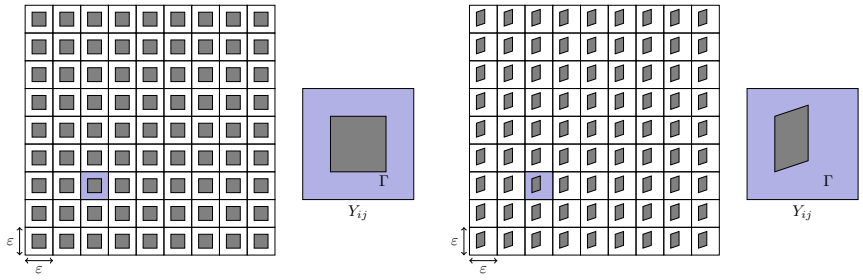

Figure 1: Microstructure of Ω^ε. Left: isotropic case; Right: anisotropic case. Here Y_{ij} is the periodic cell.

As customary in periodic homogenization applications, we introduce the fast variable $y := x/\varepsilon$ and let all the unknowns be represented by the following expansions:

$$\begin{cases} u^\varepsilon(x) & := u_0^\varepsilon(x,y) + \varepsilon u_1^\varepsilon(x,y) + \varepsilon^2 u_2^\varepsilon(x,y) + \mathcal{O}(\varepsilon^3), \\ v^\varepsilon(x) & := v_0^\varepsilon(x,y) + \varepsilon v_1^\varepsilon(x,y) + \varepsilon^2 v_2^\varepsilon(x,y) + \mathcal{O}(\varepsilon^3). \end{cases} \tag{29}$$

The asymptotic expansions (29) can be justified by means of the concept of two-scale convergence by Nguetseng and Allaire; see Ref. Krehel, Muntean, and Aiki, 2014 for the mathematical analysis of a more complex case including also thermal effects, and Hornung and Jäger, 1991 for a closely related scenario.

Now, taking into account the chain rule $\nabla := \nabla_x + \frac{1}{\varepsilon}\nabla_y$, we get:

$(0,T)$	= time interval of interest
Ω	= bounded domain in $\mathbb{R}^n$
$\partial\Omega$	= $\Gamma_R \cup \Gamma_N$ piecewise smooth boundary of Ω, $\Gamma_R \cap \Gamma_N = \emptyset$
$\vec{e}_i$	= ith unit vector in $\mathbb{R}^n$ ($n = 2$ or $n = 3$)
Y	= $\{\sum_{i=1}^n \lambda_i \vec{e}_i : \ 0 < \lambda_i < 1\}$ unit cell in $\mathbb{R}^n$
Y_0	= open subset of Y that represents the solid grain
Y_1	= $Y \setminus \overline{Y}_0$
Γ	= ∂Y_0 piecewise smooth boundary of Y_0
X^k	= $X + \sum_{i=1}^n k_i \vec{e}_i$, where $k \in \mathbb{Z}^n$ and $X \subset Y$

Table 1: ε-independent objects.

Ω_0^ε	= $\cup\{\varepsilon Y_0^k : \ Y_0^k \subset \Omega^\varepsilon, k \in \mathbb{Z}^n\}$ array of pores
Ω^ε	= $\Omega \setminus \overline{\Omega}_0^\varepsilon$ matrix skeleton
Γ^ε	= $\partial\Omega_0^\varepsilon$ pore boundaries

Table 2: ε-dependent objects.

$$\nabla u_i^\varepsilon = \varepsilon^{-1}\nabla_y u_{i,0}^\varepsilon + \varepsilon^0(\nabla_x u_{i,0}^\varepsilon + \nabla_y u_{i,1}^\varepsilon) + \varepsilon^1(\nabla_x u_{i,1}^\varepsilon + \nabla_y u_{i,2}^\varepsilon) + \mathcal{O}(\varepsilon^2).$$
$$\nabla v_i^\varepsilon = \varepsilon^{-1}\nabla_y v_{i,0}^\varepsilon + \varepsilon^0(\nabla_x v_{i,0}^\varepsilon + \nabla_y v_{i,1}^\varepsilon) + \varepsilon^1(\nabla_x v_{i,1}^\varepsilon + \nabla_y v_{i,2}^\varepsilon) + \mathcal{O}(\varepsilon^2).$$

This gives us the following diffusion term:

$$\begin{aligned}\nabla \cdot (d_i^\varepsilon(y)\nabla u_i^\varepsilon) = {} & \varepsilon^{-2}\nabla_y \cdot (d_i^\varepsilon(y)\nabla_y u_{i,0}^\varepsilon) \\ & + \varepsilon^{-1}(d_i^\varepsilon(y)\nabla_x \cdot \nabla_y u_{i,0}^\varepsilon + \nabla_y \cdot (d_i^\varepsilon(y)\nabla_x u_{i,0}^\varepsilon) + \nabla_y \cdot (d_i^\varepsilon(y)\nabla_y u_{i,1}^\varepsilon)) \\ & + \varepsilon^0(d_i^\varepsilon(y)\Delta u_{i,0}^\varepsilon + d_i^\varepsilon(y)\nabla_x \cdot \nabla_y u_{i,1}^\varepsilon \\ & \quad + \nabla_y \cdot (d_i^\varepsilon(y)\nabla_x u_{i,1}^\varepsilon) + \nabla_y \cdot (d_i^\varepsilon(y)\nabla_y u_{i,2}^\varepsilon)) + \mathcal{O}(\varepsilon^1).\end{aligned}$$

Collecting the terms with ε^{-2} gives:

$$\nabla_y \cdot (d_i^\varepsilon(y)\nabla u_{i,0}^\varepsilon) = 0.$$

Recalling that this PDE with periodic boundary conditions has a solution unique up to a constant, we get $u_{i,0}^\varepsilon = u_{i,0}^\varepsilon(x)$. Consequently, we have $\nabla_y u_{i,0}^\varepsilon = 0$.

The terms with ε^{-1} can be arranged as

$$\nabla_y \cdot (d_i^\varepsilon(y)\nabla_y u_{i,1}^\varepsilon) = -\nabla_y d_i^\varepsilon(y) \cdot \nabla_x u_{i,0}^\varepsilon. \tag{30}$$

Let $w_j(y)$ solve the following *cell problem* endowed with periodic boundary conditions:

$$\nabla_y \cdot (d_i^\varepsilon(y)\nabla w_j) = -(\nabla d_i^\varepsilon(y))_j \qquad j \in \{1,\dots,d\}, y \in Y \tag{31}$$

Using (31), we can express the first order term in (29) as:

$$u_{i,1}^{\varepsilon}(x,y) = w(y) \cdot \nabla u_{i,0}^{\varepsilon}(x) + u_{i,1}^{\varepsilon}(x), \tag{32}$$

where the function $u_{i,1}^{\varepsilon}(x)$ does not depend on the variable y. Note that

$$\nabla_y u_{i,1}^{\varepsilon}(x,y) = \nabla w(y) \cdot \nabla u_{i,0}^{\varepsilon}(x). \tag{33}$$

The terms with ε^0 give:

$$\begin{aligned}\partial_t u_{i,0}^{\varepsilon} =& d_i^{\varepsilon}(y)\Delta u_{i,0}^{\varepsilon} + d_i^{\varepsilon}(y)\nabla w(y) : \nabla\nabla u_{i,0}^{\varepsilon} \\ &+ \nabla_y \cdot (d_i^{\varepsilon}(y)\nabla_x u_{i,1}^{\varepsilon} + d_i^{\varepsilon}(y)\nabla_y u_{i,2}^{\varepsilon}) + \Lambda R_i(u_0^{\varepsilon}).\end{aligned}$$

Integrating over Y and noting that $|Y| = 1$ yield:

$$\partial_t u_{i,0}^{\varepsilon} = \bar{\mathbb{D}}_i : \nabla\nabla u_{i,0}^{\varepsilon} - \int_{\partial Y} d_i^{\varepsilon}(y)(\nabla_x u_{i,1}^{\varepsilon} + \nabla_y u_{i,2}^{\varepsilon}) \cdot n d\sigma(y) + \Lambda R_i(u_0^{\varepsilon}). \tag{34}$$

The upscaled diffusion tensors $\bar{\mathbb{D}}_i := [\bar{D}_{ijk}]$ reads:

$$\bar{D}_{ijk} = \int_Y d_i(y)(\delta_{jk} + \nabla_y w_i(y))dy \qquad i \in \{1,\dots,N\}; j,k \in \{1,\dots,d\}. \tag{35}$$

Because of the periodic boundary conditions, the active part of ∂Y is only Γ. Here we have:

$$\partial_t u_{i,0}^{\varepsilon} = \bar{\mathbb{D}}_i : \nabla\nabla u_{i,0}^{\varepsilon} - \int_{\Gamma} d_i^{\varepsilon}(y)(\nabla_x u_{i,1}^{\varepsilon} + \nabla_y u_{i,2}^{\varepsilon}) \cdot n d\sigma(y) + \Lambda R_i(u_0^{\varepsilon}). \tag{36}$$

The boundary term in (36) can be expressed recalling the corresponding deposition boundary condition:

$$-d_i^{\varepsilon}\nabla u_i^{\varepsilon} \cdot n = \varepsilon(a_i^{\varepsilon}u_i^{\varepsilon} - b_i^{\varepsilon}v_i^{\varepsilon}) \tag{37}$$

Using the prescribed asymptotic expansions, (37) becomes:

$$\begin{aligned}&-d_i^{\varepsilon}(y)(\varepsilon^{-1}\nabla_y u_{i,0}^{\varepsilon} + \varepsilon^0(\nabla_x u_{i,0}^{\varepsilon} + \nabla_y u_{i,1}^{\varepsilon}) + \varepsilon^1(\nabla_x u_{i,1}^{\varepsilon} + \nabla_y u_{i,2}^{\varepsilon})) \cdot n \\ &\quad = a_i^{\varepsilon}(y)(\varepsilon^1 u_{i,0}^{\varepsilon} + \varepsilon^2 u_{i,1}^{\varepsilon}) - b_i^{\varepsilon}(y)(\varepsilon^1 v_0^{\varepsilon} + \varepsilon^2 v_1^{\varepsilon}) + \mathcal{O}(\varepsilon^2).\end{aligned}$$

Consequently, we obtain

$$-d_i^{\varepsilon}(y)(\nabla_x u_{i,1}^{\varepsilon} + \nabla_y u_{i,2}^{\varepsilon}) \cdot n = a_i^{\varepsilon}(y)u_{i,0}^{\varepsilon} - b_i^{\varepsilon}(y)v_0^{\varepsilon}.$$

Finally, the upscaled equation for u_i^{ε} reads:

$$\partial_t u_i - \nabla \cdot (\bar{\mathbb{D}}_i \nabla u_i) + A_i u_i - B_i v_i = \Lambda R_i(\mathbf{u}). \tag{38}$$

Note that the microscopic surface exchange term turns as $\varepsilon \to 0$ into the macroscopic bulk term $A_i u_i - B_i v_i$. Furthermore, the upscaled equation for v_i^{ε} is

$$\partial_t v_i = A_i u_i - B_i v_i, \tag{39}$$

where the effective constants A_i and B_i are defined by

$$A_i := Bi \int_\Gamma a_i(y)\, d\sigma(y) \tag{40}$$

and

$$B_i := Bi \int_\Gamma b_i(y)\, d\sigma(y). \tag{41}$$

Summarizing, the upscaled system describing the macroscopic dynamics of the colloids is:

$$\partial_t u_i - \nabla \cdot (\bar{\mathbb{D}}_i \nabla u_i) + A_i u_i - B_i v_i = \Lambda R_i(\mathbf{u}) \quad \text{in } \Omega, i \in \{1, \dots, N\} \tag{42}$$

$$\partial_t v_i = A_i u_i - B_i v_i \quad \text{in } \Omega, i \in \{1, \dots, N\} \tag{43}$$

$$d_i \nabla u_i = f_i \quad \text{on } \Gamma_R, i \in \{1, \dots, N\} \tag{44}$$

$$u_i = u_{iD} \quad \text{on } \Gamma_D, i \in \{1, \dots, N\} \tag{45}$$

$$u_i(\cdot, 0) = u_i^0 \quad \text{in } \Omega, i \in \{1, \dots, N\} \tag{46}$$

$$v_i(\cdot, 0) = v_i^0 \quad \text{in } \Omega, i \in \{1, \dots, N\}. \tag{47}$$

4.2 Computation of the effective diffusion tensors $\bar{\mathbb{D}}_i = \bar{D}_{ijk}$

We rely on equation (35) to approximate the main effective transport coefficients – the effective diffusion tensors $\bar{D}_{ijk}$ responsible in this scenario for the transport of the N species of colloids. See Table 3 for a calculation example (notice the symmetry of the tensors corresponding to the isotropic case).

Figure 2 and Figure 3 show the solutions to the cell problems (31) for the isotropic and anisotropic geometry case, respectively. The 2D solver for elliptic PDE with periodic boundary conditions needed for these periodic cell problems was implemented in C++ using `deal.II` Numerics library; see Bangerth et al., 2013 for details on this platform.

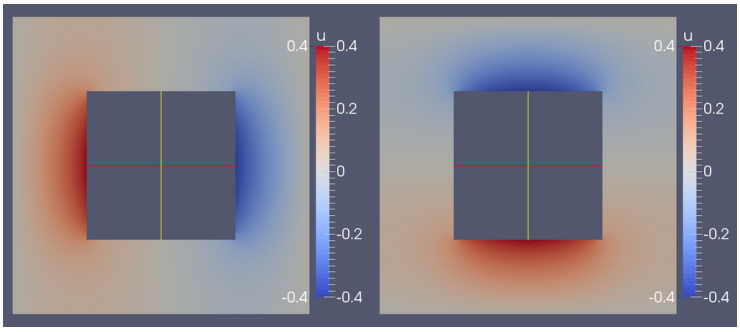

Figure 2: Solutions to the cell problems that correspond to isotropic periodic geometry (Figure 1, left). See Table 3 for the resulting effective diffusion tensor.

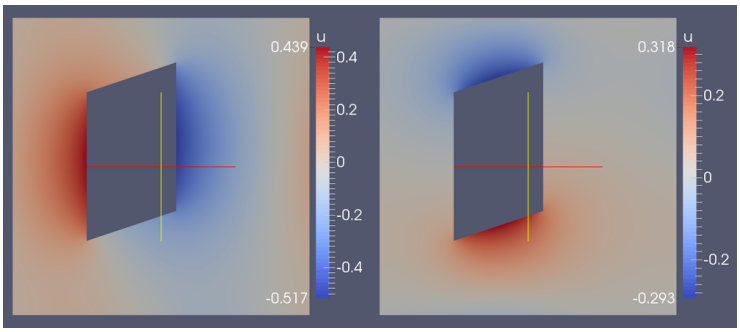

Figure 3: Solutions to the cell problems that correspond to anisotropic periodic geometry (Figure 1, right). See Table 3 for the resulting effective diffusion tensor.

Isotropic	Anisotropic
$\bar{\mathbb{D}}_1 = \begin{bmatrix} 0.75 & 0.171476 \\ 0.171476 & 0.75 \end{bmatrix}$	$\bar{\mathbb{D}}_1 = \begin{bmatrix} 0.817467 & 0.0786338 \\ 0.214942 & 0.817467 \end{bmatrix}$

Table 3: Examples of effective diffusion tensors corresponding to the first species (i.e. to the monomer population) for the two choices of microstructures shown in Figure 1.

Controlling the cell functions allows us also to approximate the tortuosity tensor in a direct manner, avoiding complex analytical calculations hard to justify theoretically or experimentally; compare e.g. with Ref. Guo, 2012. An example in this sense is shown in Figure 4. To obtain it, we use the relation

$$\bar{\mathbb{D}}_1 = d_1 \phi \bar{\mathbb{T}}^*$$

(see Bear, 1988, e.g.) and the fact that for the microstructures shown in Figure 1 we know that the porosity for the isotropic case is 0.75, while the porosity for the anisotropic case amounts to 0.85. We refer the reader to Ijioma, 2014 for more numerical examples of multiscale investigations of anisotropy effects on transport in periodically perforated media.

Isotropic	Anisotropic
$\bar{\mathbb{T}}^* = \begin{bmatrix} 1.0000 & 0.2286 \\ 0.2286 & 1.0000 \end{bmatrix}$	$\bar{\mathbb{T}}^* = \begin{bmatrix} 0.9617 & 0.0925 \\ 0.2529 & 0.9617 \end{bmatrix}$

Table 4: Examples of effective tortuosity tensors corresponding to the first species (i.e. the monomer population) for the two choices of microstructures shown in Figure 1.

As soon as the covering with microstructures lacks ergodicity and/or station-

arity, such evaluations are often replaced by efforts to calculate accurate upper bounds on the prominent effective coefficients; see Ref. Mei and Vernescu, 2012, for instance, for details in this direction.

4.3 Extensions to non-periodic microstructures

One can relax the periodicity assumption on the distribution of the microstructures. Instead of promoting the stochastic homogenization approach (cf. Ref. Zhikov, 2000, e.g.) which is prohibitory expensive from the computational point of view, we indicate two computationally tractable cases: (1) the locally periodic arrays of microstructures (see Boyaval, 2008; Fatima et al., 2011; Muntean and van Noorden, 2013) and (2) the weakly stochastic case (see Le Bris, Legoll, and Thomines, 2014 and references cited therein). We will show elsewhere not only how our model formulation and asymptotics as $\varepsilon \to 0$ translate into the frameworks of these two non-periodic settings, but also the way the new effective transport coefficients can be approximated numerically.

5 Simulation studies

In this section, we study how aggregation affects deposition during the transport of colloids in porous media. Within this frame we work with a reference parameter regime pointing out to the *fast aggregation – slow deposition regime*, that is high Λ and low Bi.

We take the model from Johnson, Sun, and Elimelech, 1996 as the starting point of this discussion and aim at recovering their results. We interpret all coefficients from Johnson, Sun, and Elimelech, 1996 in terms of our effective coefficients obtained by the asymptotic homogenization performed in Section 4. As main task, we search for new effects coming into play due to colloids aggregation.

The model for the evolution of the single mobile colloid species $n(x,t)$ and the surface coverage of the porous matrix by the immobile colloids $\theta(x,t)$ (that corresponds to the amount of mass deposited) is as follows: Find the pair (n,θ) satisfying the balance equations

$$\partial_t n = -v_p \cdot \nabla n + D_h \Delta n - \frac{f}{\pi a_p^2} \partial_t \theta, \tag{48}$$

$$\partial_t \theta = \pi a_p^2 k n B(\theta), \tag{49}$$

with the switch boundary conditions

$$n(t,0) = \begin{cases} n_0 & t \in [0,t_0] \\ 0 & t > t_0 \end{cases}, \tag{50}$$

$$\frac{\partial n}{\partial \nu}(t,L) = 0, \tag{51}$$

and initial conditions

$$n(0,x) = 0, \tag{52}$$
$$\theta(0,x) = 0,\ x \in [0,L]. \tag{53}$$

Here v_p is the interstitial particle velocity of the suspended colloids, D_h is the hydrodynamic particle dispersion, a_p is the particle radius, while f is the specific surface area. t_0 is the switching off time in the boundary condition.

Given a column of cross-section surface S and height Z randomly packed with spherical collector beads of radius a_c and porosity (void volume fraction) ϕ typically of order of 0.4, f can be calculated (cf. Privman et al., 1991) as the ratio of the total surface area of all beads in the column to the void volume ϕZS. For spherical beads of uniform radius, the specific surface area f is

$$f(\phi) := \frac{3(1-\phi)}{\phi a_c}. \tag{54}$$

The dynamic blocking function $B(\theta)$ arising in (49) accounts for the transient rate of particle deposition. As the colloids accumulate on the surface of the porous matrix, they exclude a part of the surface, limiting the amount of sites for further particle attachment.

Interstitial particle velocity	$v_p = \frac{U}{\phi}(2 - (1 - \frac{a_p}{r_0})^2)$
Hydrodynamic dispersion coefficient	$D_h = \frac{D_\infty}{\tau} + \alpha_L v_p$
Particle radius	$a_p = 0.15\,[\mu m]$
Specific surface area	$f = \frac{3(1-\phi)}{\phi a_c}$
Collector grain radius	$a_c = 0.16\,[mm]$
Pore radius	$r_0 = (1.1969\varepsilon - 0.1557)a_c$
Darcy velocity	$U = 1.02 \times 10^{-4}\,[m/s]$
Porosity	$\phi = 0.392\,[-]$
Dispersivity parameter	$\alpha_L = 0.692\,[mm]$
Kinetic rate constant	$k = 0.25\eta U = 5 \times 10^{-7}\,[m/s]$
Characteristic length	$L = 0.101\,[m]$
Characteristic time	$t_0 = 5445\,[s]$
Initial concentration	$n_0 = 5.58 \times 10^8\,[cm^{-3}]$

Table 5: Reference parameters for simulation studies. The numerical values are taken from Johnson, Sun, and Elimelech, 1996.

We used the Finite Element Numerics toolbox DUNE Bastian et al., 2008 to implement a solver for the model. We employed the Newton method to deal with the nonlinearities in the aggregation term (counterpart of $R(\cdot)$ cf. Section 2.1) and in the blocking function term (here denoted by $B(\cdot)$). An implicit Euler iteration is used for time-stepping.

The first results of our simulation with the reference parameters indicated in Table 5 are shown in Figure 4. Essentially, a single-species system (48)-(53) is compared to a two-species system with a square pulse going from one side of the domain for a fixed amount of time in the first species only. The resulting breakthrough curves are plotted. It is of interest to compare the breakthrough curves for the total amount of mass going through, no matter if it's in the form of small or large particles. As we can observe, there is a perceptible difference between the two curves, being the mass for the two-species case coming in slower. This is due to larger particles having higher affinity for deposition.

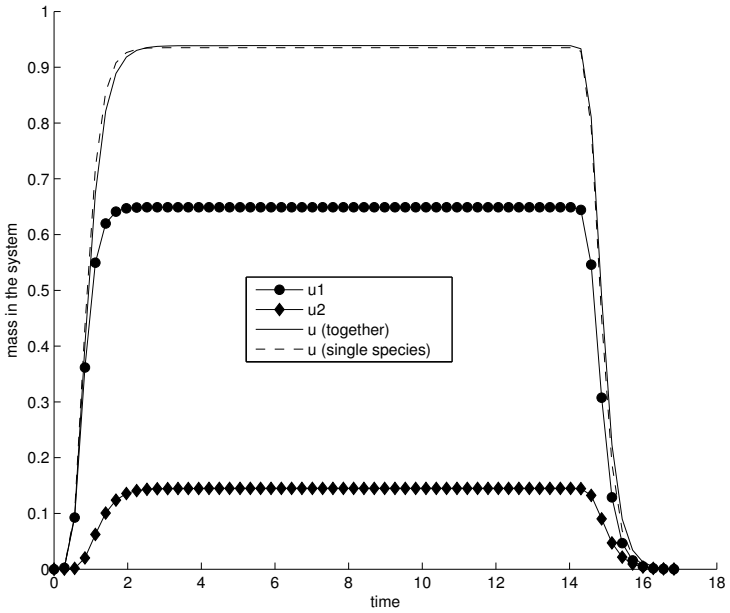

Figure 4: Simulation comparison for a single species system *versus* an aggregating system. The straight line is the breakthrough curve for the colloidal mass for the problem without aggregation. The dashed line is the breakthrough curve for the colloidal mass for the problem with aggregation. It is obtained by summing mass-wise the breakthrough curves for the monomers u_1 and dimers u_2.

Let us focus now our attention on a specific aspect of the deposition process, namely on the effect of the dynamic blocking functions. The context is as follows: The rate of colloidal deposition is known to go down as more particles attach themselves the the favorable deposition sites of the porous matrix; see, for instance, Liu, Johnson, and Elimelech, 1995 and references cited therein.

One of the choices for the blocking function in (49) corresponds to Langmuir's molecular adsorption model Langmuir, 1918. It is an affine function in terms of θ, reaching the maximum of 1 when the fraction of the surface covered

is zero. In other words, $B(\cdot)$ is defined as

$$B(\theta) := 1 - \beta\theta. \tag{55}$$

For the simulations, we used the value $\beta = 2.9$. This corresponds to the hard sphere jamming limit $\theta_\infty = 0.345$, which is specific to spherical collector geometry and the experimental conditions described in Johnson and Elimelech, 1995.

A simulation example of our balance equations (48)-(53) with the Langmuirian blocking function is shown in Figure 5.

Another choice is the RSA dynamic blocking function as developed in Schaaf and Talbot, 1989. RSA stands for "random sequential adsorption". The RSA blocking choice is based on a third order expansion of excluded area effects and can be used for low and moderate surface coverage. Here $B(\theta)$ is defined as:

$$B(\theta) := 1 - 4\theta_\infty\beta\theta + 3.308(\theta_\infty\beta\theta)^2 + 1.4069(\theta_\infty\beta\theta)^3. \tag{56}$$

Here, θ_∞ is the hard sphere jamming limit. A simulation example of the balance equations (48)-(53) including the RSA blocking function is shown in Figure 6.

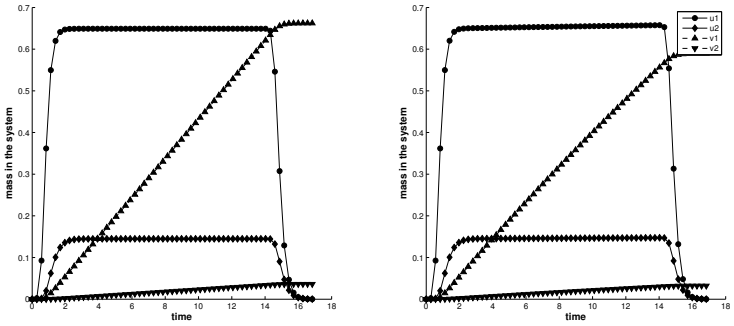

Figure 5: The effect of the Langmuirian dynamic blocking function on the deposition (right) *versus* no blocking function (left). u_1 and u_2 are the breakthrough curves, while v_1 and v_2 are the concentrations of the deposited species.

6 Discussion

This paper sheds light on transport, aggregation/flocculation, and deposition of colloidal particles in heterogeneous media. We succeeded to recover basic results obtained with standard models for (single class, single species) colloidal transport. Furthermore, our model includes information about the multiscale structure of the porous medium and demonstrates new effects attributed to flocculation, such as the occurrence of an overall decrease in the species mobility due to a higher affinity for deposition of the large size classes of colloidal species; see Figure 7 for this effect.

Extensions of this work can go in multiple directions:

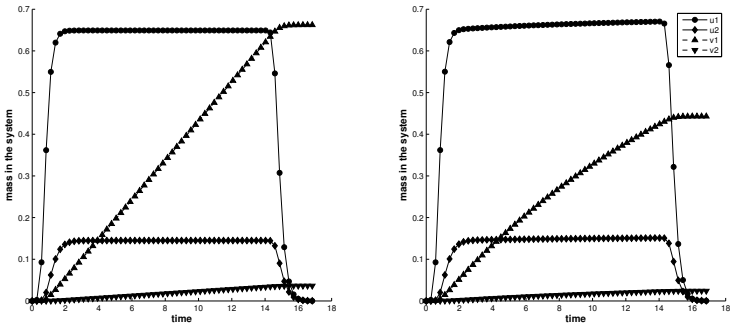

Figure 6: The effect of the RSA dynamic blocking function on the deposition (right) *versus* no blocking function (left). u_1 and u_2 are the breakthrough curves, while v_1 and v_2 are the concentrations of the deposited species.

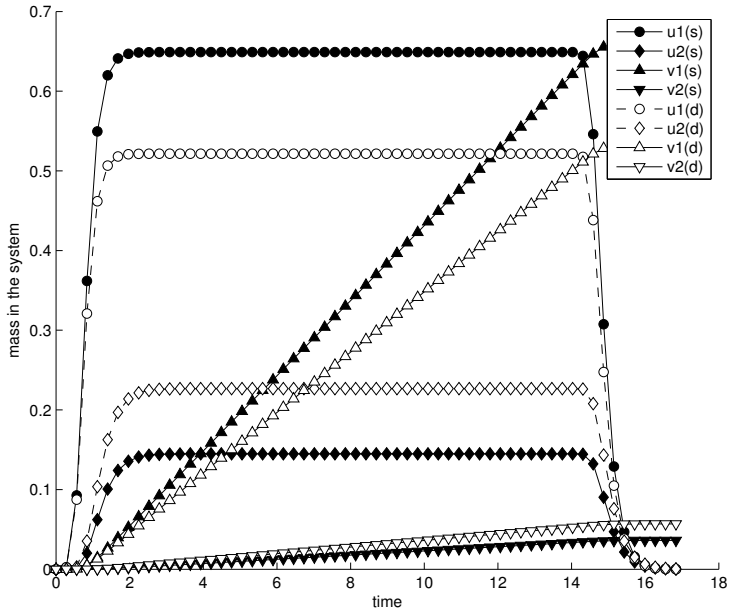

Figure 7: The effect of aggregation rates on the breakthrough curves. On the left, the default rate of aggregation is used, on the right - it's doubled. A change of aggregation rate can be achieved by varying the concentration of salt in the suspension, according to DLVO theory. Note the strong effect of aggregation on deposition.

(i) Cf. Liu, Johnson, and Elimelech, 1995, the extent of colloidal transport in groundwater is largely determined by the rate at which colloids deposit on stationary grain surfaces. The assumption of stationarity can

be potentially relaxed, thus aiming to incorporate the interplay between biofilms growth and deposition, hence obtaining a better understanding of the clogging/blocking of the pores; see e.g. Noorden et al., 2010; Ray et al., 2013.

(ii) If repulsive forces between colloids are absent due to suitable chemical conditions, then the deposition rate tends to increase as colloids accumulate on the grain surface (see Figure 1). Based on Liu, Johnson, and Elimelech, 1995, this enhancement of deposition kinetics is attributed to the retained particles and is generally referred to as ripening. Active repulsive forces seem to lead to a decline in the deposition kinetics. These effects could be investigated by our model, provided suitable modifications of the fluxes responsible for the transport of colloidal species are taken into account Hertz and Knabner, 2013.

(iii) The role of the electrolyte concentration (typically a salt, e.g. KCl) and the effect of the interplay between the electrostatic and van der Waals interactions on deposition kinetics can be studied by further developing the model. A few basic ideas on how to proceed in this case are collected, for instance, in Ray, Muntean, and Knabner, 2012.

(iv) Non-periodic distributions of microstructures are relevant for practical applications. We leave as further work the extension of our solver towards the MsFEM approach, where cell problems are solved for each grid element, parametrized by the localized properties of the medium. We refer the reader to Section 4.3 for comments in this direction.

Acknowledgments

The authors would like to thank Prof. Dr. Kai Uwe Totsche (Jena) and his group for very helpful discussions on the complexity of the interactions and transport of colloids in soils.

AM and OK gratefully acknowledge financial support by the European Union through the Initial Training Network *Fronts and Interfaces in Science and Technology* of the Seventh Framework Programme (grant agreement number 238702).

References

Bangerth, W. et al. (2013). "The `deal.II` Library, Version 8.1". In: *arXiv preprint* *http://arxiv.org/abs/1312.2266v4*.

Bastian, P. et al. (2008). "A generic grid interface for parallel and adaptive scientific computing. Part II: implementation and tests in DUNE". En. In: ISSN: 1436-5057. URL: `http://dx.doi.org/10.1007/s00607-008-0004-9`.

Battino, R. and H. L. Clever (1966). "The solubility of gases in liquids". In: *Chemical Reviews* 66.4, pp. 395–463.

Bear, J. (1988). *Dynamics of Fluids in Porous Media*. Dover.

Bensoussan, A., J. L. Lions, and G. Papanicolaou (1978). *Asymptotic Analysis for Periodic Structures*. Vol. 5. Studies in Mathematics and Its Applications. North-Holland.

Boyaval, S. (2008). "Reduced-basis approach for homogenization beyond the periodic setting". In: *SIAM Multiscale Modeling and Simulation* 7.1, pp. 466–494.

Camejo, C. C., R. Gröpler, and G. Warnecke (2012). "Existence and uniqueness of solutions to the coagulation equations with singular kernel". In: *arXiv preprint arXiv:1210.1500*.

Chechkin, G. A., A. L. Piatnitki, and A. S. Shamaev (2007). *Homogenization Methods and Applications*. Vol. 234. Translations of Mathematical Monographs. Providence, Rhode Island: AMS.

Derjaguin, B. and L. Landau (1941). "A theory of the stability of strongly charged lyophobic sols and the coalescence of strongly charged particles in electrolytic solution". In: *Acta Phys.-Chim. USSR* 14, pp. 633–662.

Elimelech, M. et al. (1995). *Particle Deposition and Aggregation: Measurement, Modelling and Simulation*. Elsevier.

Fatima, T. et al. (2011). "Homogenization of a reaction–diffusion system modeling sulfate corrosion of concrete in locally periodic perforated domains". In: *Journal of Engineering Mathematics* 69.2-3, pp. 261–276.

Guo, P. (2012). "Dependency of tortuosity and permeability of porous media on directional distribution of pore voids". In: *Transport in Porous Media* 95.2, pp. 285–303.

Hamaker, H.C. (1937). "The London - van der Waals attraction between spherical particles". In: *Physica* 4.10, pp. 1058–1072.

Hertz, M. and P. Knabner (2013). *Including van der Waals forces in diffusion-convection equations - modeling, analysis, and numerical simulations*. Tech. rep. No. 373. Erlangen: Institute for Applied Mathematics.

Hornung, U. and W. Jäger (1991). "Diffusion, convection, adsorption, and reaction of chemicals in porous media". In: *Journal of Differential Equations* 92.2, pp. 199–225.

Ijioma, E. (2014). "Homogenization approach to filtration combustion of reactive porous materials: modelling, simulation, analysis". PhD thesis. Tokyo, Japan: University of Meiji.

Johnson, P. R. and M. Elimelech (1995). "Dynamics of colloid deposition in porous media: Blocking based on random sequential adsorption". In: *Langmuir* 11.3, pp. 801–812.

Johnson, P. R., N. Sun, and M. Elimelech (1996). "Colloid transport in geochemically heterogeneous porous media: Modeling and measurements". In: *Environ. Sci. Techn.* 30.11, pp. 3284–3293.

Knabner, P., K.U. Totsche, and I. Kögel-Knabner (1996). "The modeling of reactive solute transport with sorption to mobile and immobile sorbents: 1. Experimental evidence and model development". In: *Water Resources Research* 32.6, pp. 1611–1622.

Krehel, O., A. Muntean, and T. Aiki (2014). *A thermo-diffusion system with Smoluchowski interactions: well-posedness and homogenization*. Tech. rep. No. 14-09. Eindhoven: CASA Report, TU/e.

Krehel, O., A. Muntean, and P. Knabner (2012). "On modeling and simulation of flocculation in porous media". In: *Proceedings of XIX International Conference on Water Resources in Urbana, IL*.

Langmuir, I. (1918). "The adsorption of gases on plane surfaces of glass, mica and platinum." In: *Journal of the American Chemical society* 40.9, pp. 1361–1403.

Le Bris, C., F. Legoll, and F. Thomines (2014). "Multiscale Finite Element approach for weakly random problems and related issues". In: *M2AN* (to appear).

Lith, B.S. van, S. Storm, and A. Muntean (2013). *A multiscale model for self-assembly with secondary nucleation-like properties*. Tech. rep. No. 13-06. Eindhoven: CASA Report. TU/e.

Liu, D., P. R. Johnson, and M. Elimelech (1995). "Colloid deposition dynamics in flow-through porous media: Role of electrolyte concentration". In: *Environ. Sci. Techn.* 29.12, pp. 2963–2973.

Marchenko, V. A. and E. Y. Kruslov (2006). *Homogenization of Partial Differential Equations*. Birkhäuser.

Meakin, P. (1987). "Fractal aggregates". In: *Adv. Colloid Interface Sci.* 28, pp. 249–331.

Mei, C. C. and B. Vernescu (2012). *Dynamics of Fluids in Porous Media*. World Scientific.

Muntean, A. and T. L. van Noorden (Oct. 2013). "Corrector estimates for the homogenization of a locally periodic medium with areas of low and high diffusivity". In: *Eur. J. Appl. Math.* 24 (05), pp. 657–677.

Muntean, A. et al. (2014). "Pedestrians moving in the dark: Balancing measures and playing games on lattices". In: *Collective Dynamics from Bacteria to Crowds: An Excursion Through Modeling, Analysis and Simulation*. Ed. by A. Muntean and F. Toschi. Vol. 553. CISM Courses and Lectures. Berlin: Springer Verlag, pp. 75–104.

Noorden, T. L. van et al. (2010). "An upscaled model for biofilm growth in a thin strip". In: *Water Resources Research* 46.6.

Nordbotten, J. M. and M. A. Celia (2012). *Geological Storage of CO2: Modeling Approaches for Large-Scale Simulation*. Willey.

Peukert, W., H.C. Schwarzer, and F. Stenger (2005). "Control of aggregation in production and handling of nanoparticles". In: *Chemical Engineering and Processing* 44.2, pp. 245–252.

Privman, V. et al. (1991). "Particle adhesion in model systems. Part 13. Theory of multilayer deposition". In: *J. Chem. Soc., Faraday Trans.* 87.9, pp. 1371–1375.

Ray, N., A Muntean, and P. Knabner (2012). "Rigorous homogenization of a Stokes–Nernst–Planck–Poisson system". In: *Journal of Mathematical Analysis and Applications* 390.1, pp. 374–393.

Ray, N. et al. (2013). "Drug release from collagen matrices including an evolving microstructure". In: *ZAMM – Zeitschrift für Angewandte Mathematik und Mechanik* 93.10-11, pp. 811–822.

Rosenholm, J. M., C. Sahlgren, and M. Lindén (2010). "Towards multifunctional, targeted drug delivery systems using mesoporous silica nanoparticles–opportunities & challenges". In: *Nanoscale* 2.10, pp. 1870–1883.

Schaaf, P. and J. Talbot (1989). "Surface exclusion effects in adsorption processes". In: *The Journal of Chemical Physics* 91.7, pp. 4401–4409.

Smoluchowski, M. (1917). "Versuch einer mathematischen Theorie der Koagulationskinetik kolloider Lösungen". In: *Z. Phys. Chem* 92, pp. 129–168.

Totsche, K. U. and I. Kögel-Knabner (2004). "Mobile organic sorbent affected contaminant transport in soil". In: *Vadose Zone Journal* 3.2, pp. 352–367.

Totsche, K.U., P. Knabner, and L. Kögel-Knabner (1996). "The modeling of reactive solute transport with sorption to mobile and immobile sorbents: 2. Model discussion and numerical simulation". In: *Water Resources Research* 32.6, pp. 1623–1634.

Zhikov, V. V. (2000). "On an extension of the method of two-scale convergence and its applications". In: *Sb. Math.* 191, p. 973.

PREVIOUS PUBLICATIONS IN THIS SERIES:

Number	Author(s)	Title	Month
14-08	A. Corbetta A. Muntean F. Toschi K. Vafayi	Parameter estimation of social forces in crowd dynamics models via a probabilistic method	March '14
14-09	O. Krehel A. Muntean T. Aiki	A thermo-diffusion system with Smoluchowski interactions: well-posedness and homogenization	Apr. '14
14-10	N. Banagaaya G. Ali W.H.A. Schilders	Implicit-IMOR method for index-1 and index-2 linear constant DAEs	Apr. '14
14-11	M.H. Duong M. Fathi	The two-scale approach to hydrodynamic limits for non-reversible dynamics	Apr. '14
14-12	O. Krehel A. Muntean P. Knabner	Multiscale modeling of colloidal dynamics in porous media: Capturing aggregation and deposition effects	Apr. '14

Ontwerp: de Tantes,
Tobias Baanders, CWI